Supporting information

Anti-site reordering in $LiFePO_4$:
Defect annihilation on charge carrier injection

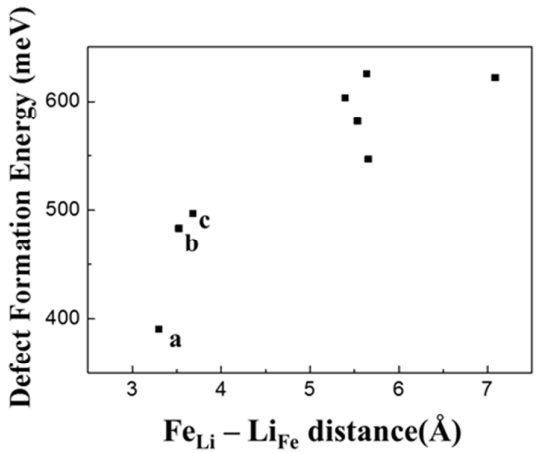

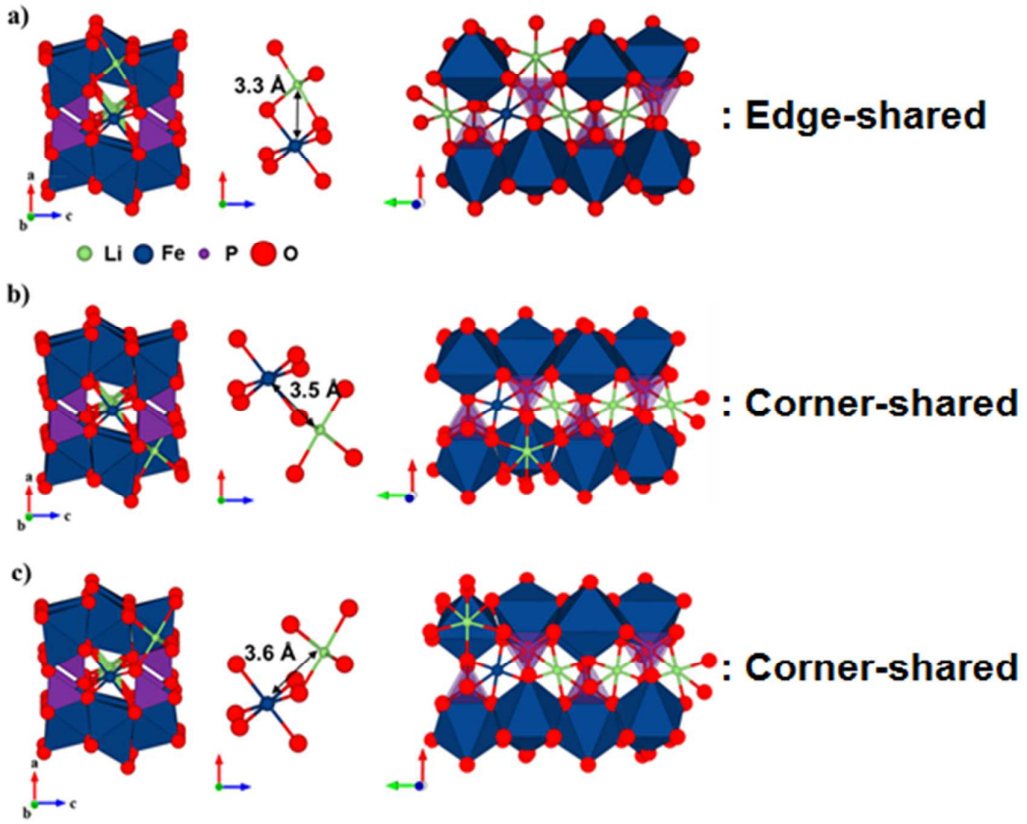

Figure S1. Calculated formation energy of anti-site defect in $LiFePO_4$ and its configuration corresponding to the distance between Li^+ on Fe^{2+} site and Fe^{2+} on Li^+ site. Near anti-site defect has lower formation energy. (a) Edge-shared anti-site defect with the lowest formation energy (about 390 meV) (b), (c) Corner-shared anti-site defect with the formation energy of about 490 meV.

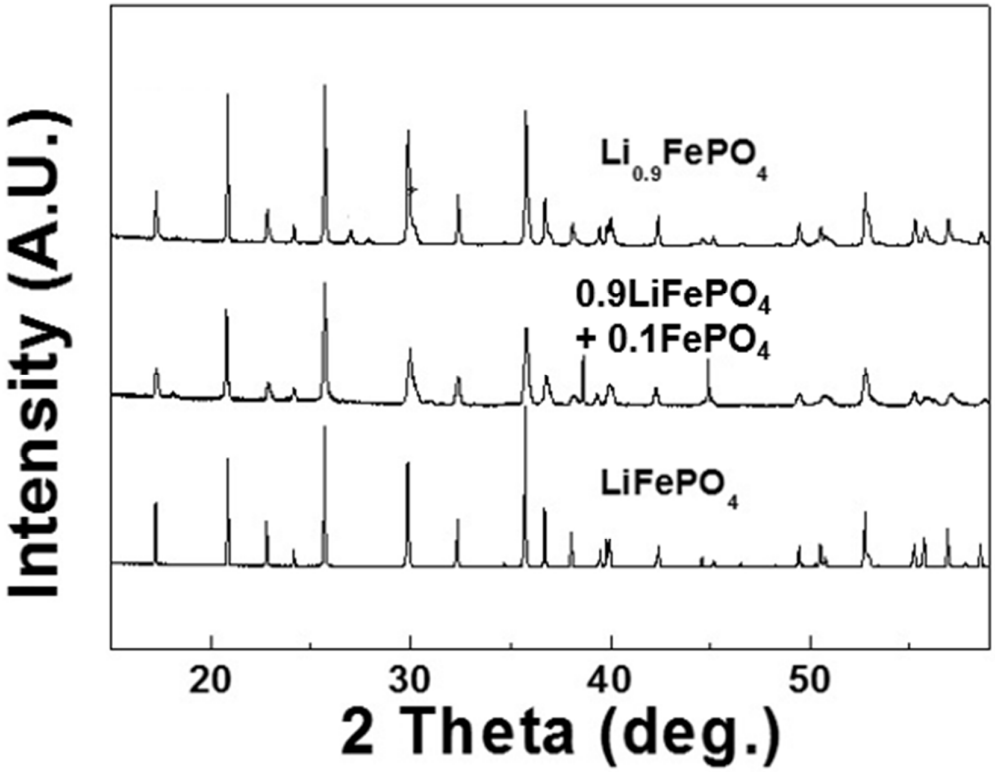

Figure S2. The 15 ~ 55° high resolution powder diffraction patterns of prepared by hydrothermal synthesis.

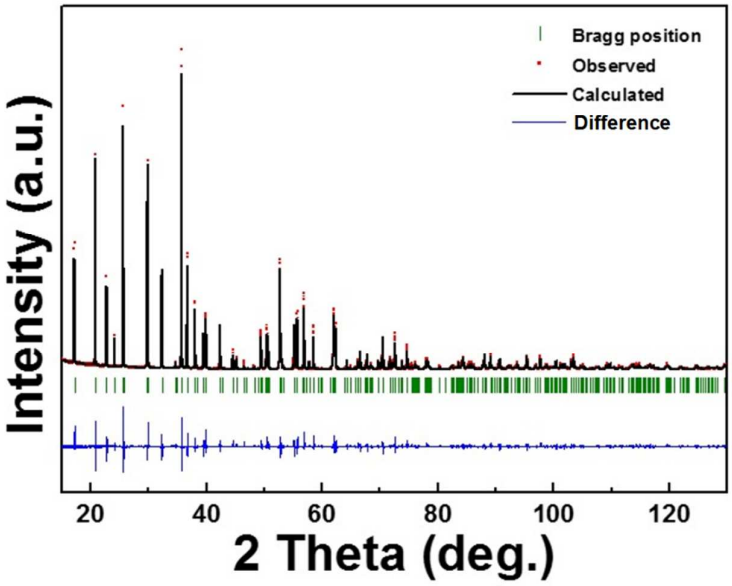

Atom	X	Y	Z	Biso	Mult.	Occ.		
Li	0.00000(0)	0.00000(0)	0.00000(0)	1.49	4	0.479	**Chi^2**	5.49
Fe	0.28189(7)	0.25000(0)	0.97522(17)	0.395	4	0.479	**R_p**	11
Li_{Fe}	0.28189(7)	0.25000(0)	0.97522(17)	1.49	4	0.021	**R_I**	5.02
Fe_{Li}	0.00000(0)	0.00000(0)	0.00000(0)	0.395	4	0.021	**R_f**	3.44
P	0.09524(13)	0.25000(0)	0.41750(26)	0.282	4	0.500	**Unit cell V.**	292.640(1)
O1	0.09721(34)	0.25000(0)	0.74437(64)	0.495	4	0.500	**Lattice a(Å)**	10.35027(3)
O2	0.45596(36)	0.25000(0)	0.20695(65)	0.482	4	0.500	**Lattice b(Å)**	6.01304(2)
O3	0.16747(28)	0.04299(38)	0.28245(42)	0.518	8	1.000	**Lattice b(Å)**	4.70205(1)

Figure S3. Rietveld refinement results of hydrothermally prepared $LiFePO_4$.

Atom	X	Y	Z	Biso	Mult.	Occ.		
Li	0.00000(0)	0.00000(0)	0.00000(0)	1.49	4	0.430	**Chi^2**	9.65
Fe	0.28139(13)	0.25000(0)	0.97462(35)	0.395	4	0.480	**R_p**	14.2
Li_{Fe}	0.28139(13)	0.25000(0)	0.97462(35)	1.49	4	0.020	**R_I**	7.71
Fe_{Li}	0.00000(0)	0.00000(0)	0.00000(0)	0.395	4	0.020	**R_f**	4.71
P	0.09592(23)	0.25000(0)	0.41781(48)	0.282	4	0.500	**Unit cell V.**	291.998(5)
O1	0.10082(60)	0.25000(0)	0.74909(113)	0.495	4	0.500	**Lattice a(Å)**	10.32877(8)
O2	0.45482(66)	0.25000(0)	0.20070(109)	0.482	4	0.500	**Lattice b(Å)**	6.00752(6)
O3	0.16566(49	0.03936(72)	0.27621(71)	0.518	8	1.000	**Lattice b(Å)**	4.70582(4)

Figure S4. Rietveld refinement results of solid-solution $Li_{0.9}FePO_4$.

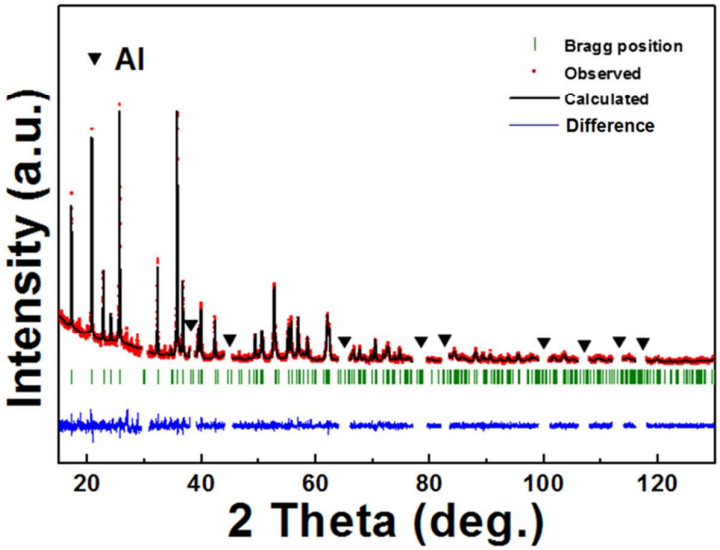

Atom	X	Y	Z	Biso	Mult.	Occ.		
Li	0.00000(0)	0.00000(0)	0.00000(0)	1.375(90)	4	0.4907(8)	Chi^2	1.50
Fe	0.28166(15)	0.25000(0)	0.97498(43)	0.369(20)	4	0.4907(8)	R_p	6.67
Li_{Fe}	0.28166(15)	0.25000(0)	0.97498(43)	0.280(90)	4	0.0093(8)	R_I	3.94
Fe_{Li}	0.00000(0)	0.00000(0)	0.00000(0)	1.464(20)	4	0.0093(8)	R_f	2.74
P	0.09816(29)	0.25000(0)	0.41935(49)	0.356(41)	4	0.500	Unit cell V.	290.637(4)
O1	0.09531(71)	0.25000(0)	0.74595(118)	0.590(142)	4	0.500	Lattice a(Å)	10.32416(8)
O2	0.44798(82)	0.25000(0)	0.21221(109)	0.192(126)	4	0.500	Lattice b(Å)	5.99040(6)
O3	0.16480(53)	0.04815(79)	0.28282(81)	0.676(90)	8	1.000	Lattice b(Å)	4.66938(4)

Figure S5. Rietveld's refinement results of electrochemically treated $LiFePO_4$

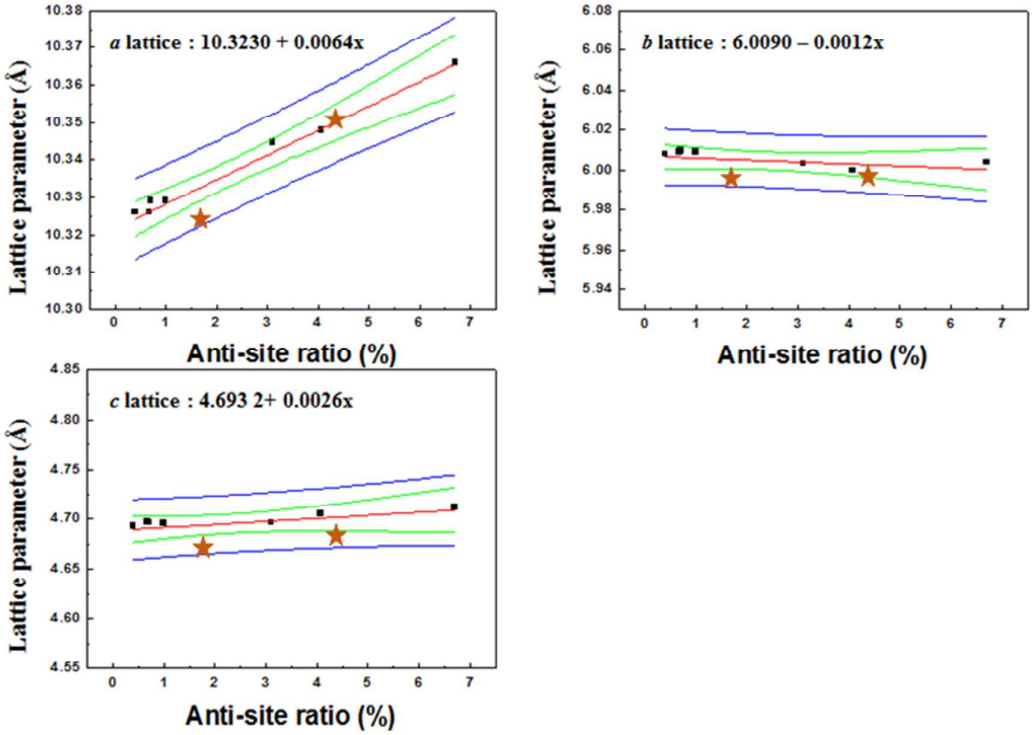

Figure S6. Lattice parameter with change modification with anti-site ratio at room temperature. Red line : trend line, blue line : confidence band, green line : prediction band. The interval coverage probability is set as 95 %. This figure used reference number 11, 18, 27 and 29.

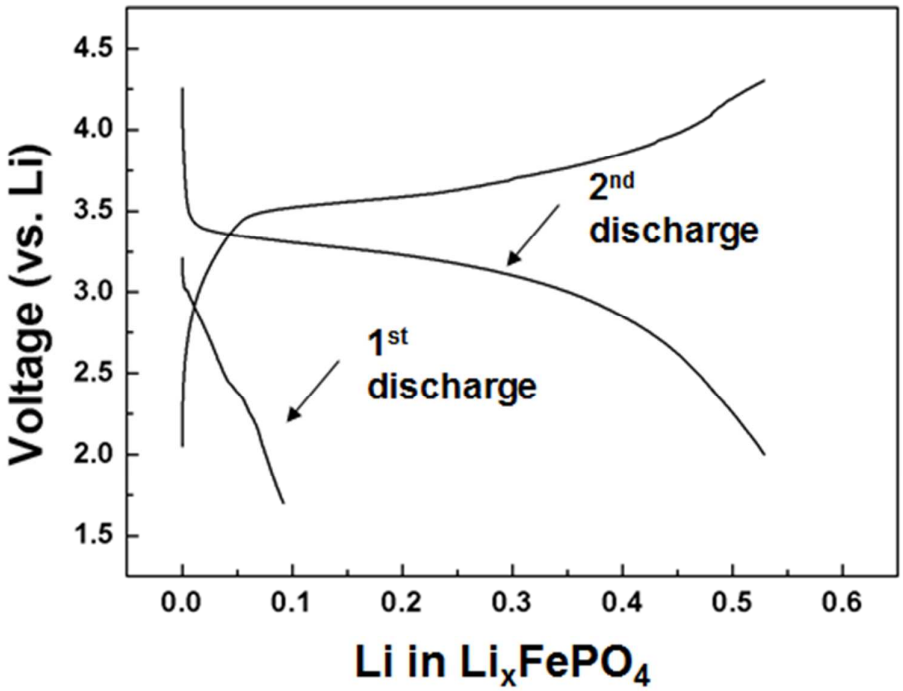

Figure S7. The electrochemical profile of solid-solution $Li_{0.9}FePO_4$ at C/100. The 1st discharge profile showed unexpected high polarization, however, the 2nd profile did not show overpotential during charging/discharging

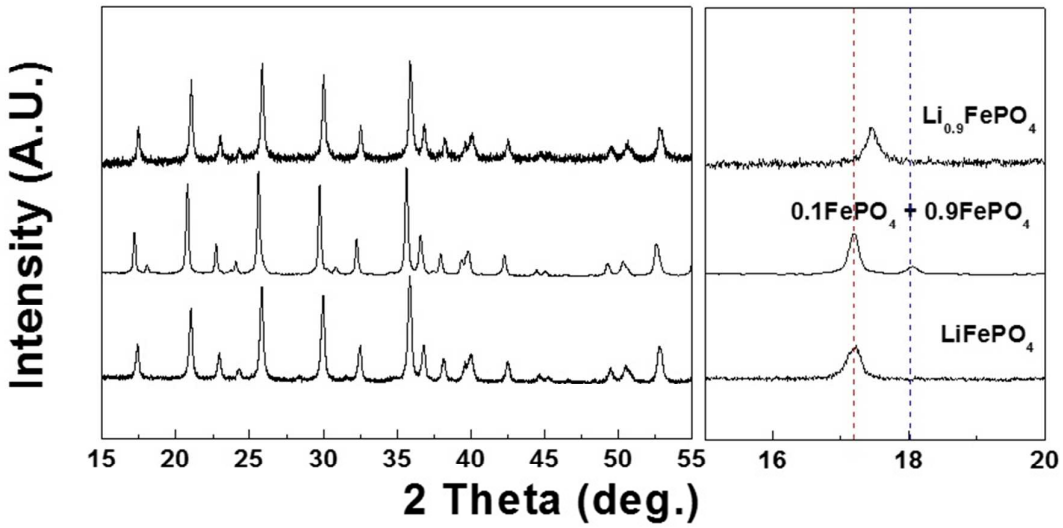

Figure S8. 15 ~ 55° XRD patterns of prepared by solid-state method samples (left) and magnified (200) peak of samples (right). red line : (200) peak of $LiFePO_4$, blue line : (200) peak of $FePO_4$. All samples are well synthesized without remarkable impurities.

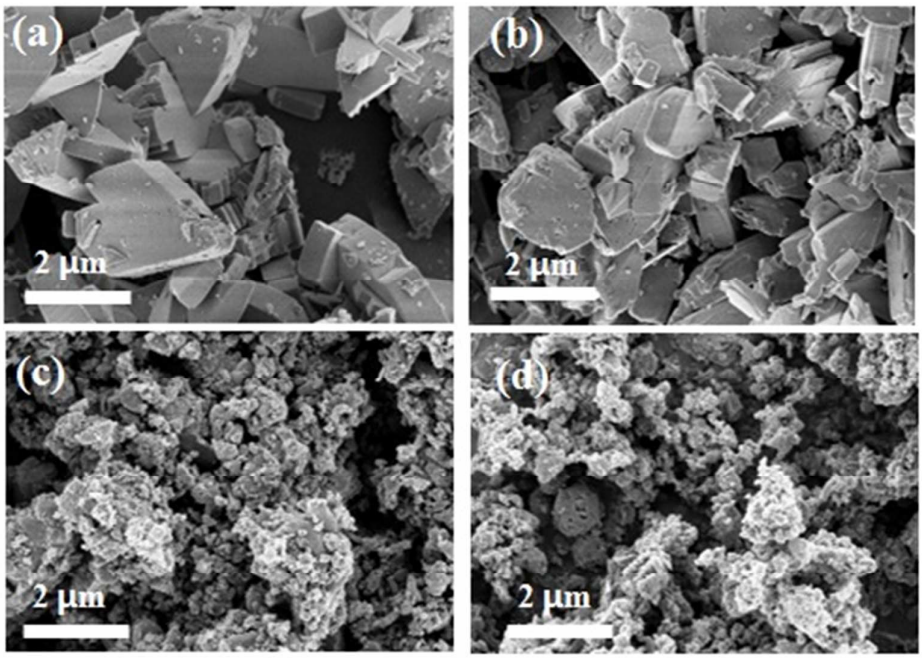

Figure S9. SEM image of prepared $LiFePO_4$. (a) Hydrothermal synthesis $LiFePO_4$ (b) 380 °C heated hydrothermal synthesis $Li_{0.9}FePO_4$ (c) 600 °C solid-state synthesis $LiFePO_4$ (d) 380 °C heated solid-state 600 °C synthesis $Li_{0.9}FePO_4$.

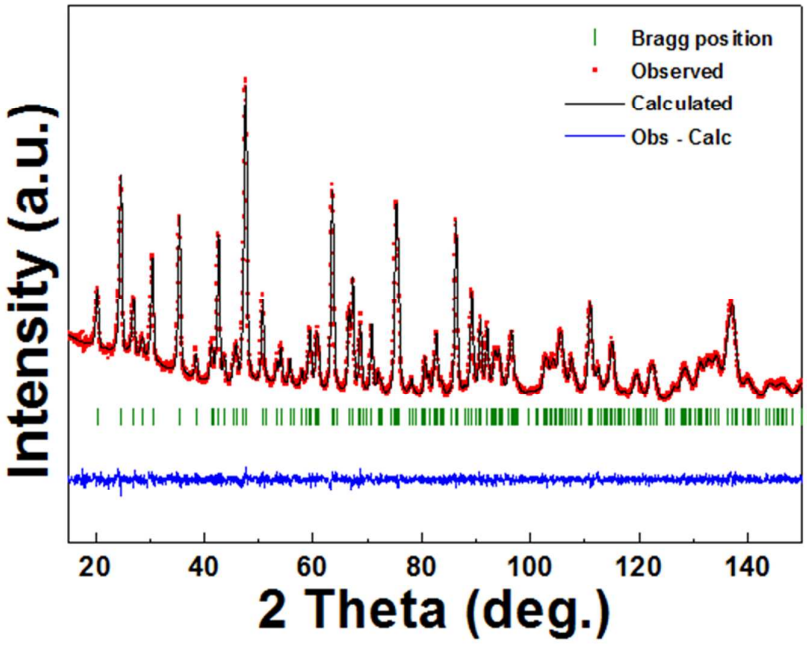

Atom	X	Y	Z	Multi.	Occ.		
Li	0.00000(0)	0.00000(0)	0.00000(0)	4	0.904(1)	Chi^2	1.24
Fe	0.28237(8)	0.25000(0)	0.9722(3)	4	0.994(1)	R_p	2.11
Li_{Fe}	0.28237(8)	0.25000(0)	0.9722(3)	4	0.006(1)	R_I	2.66
Fe_{Li}	0.00000(0)	0.00000(0)	0.00000(0)	4	0.006(1)	R_f	2.39
P	0.09444(16)	0.25000(0)	0.4191(3)	4	0.5	Unit cell V.	291.277(24)
O1	0.09832(17)	0.25000(0)	0.7403(3)	4	0.5	Lattice a(Å)	10.32029(49)
O2	0.45743(13)	0.25000(0)	0.2057(3)	4	0.5	Lattice b(Å)	6.00628(30)
O3	0.16387(12)	0.04723(18)	0.2848(2)	8	1	Lattice b(Å)	4.69903(21)

Figure S10. Neutron Rietveld refinement results of solid-state prepared $LiFePO_4$.

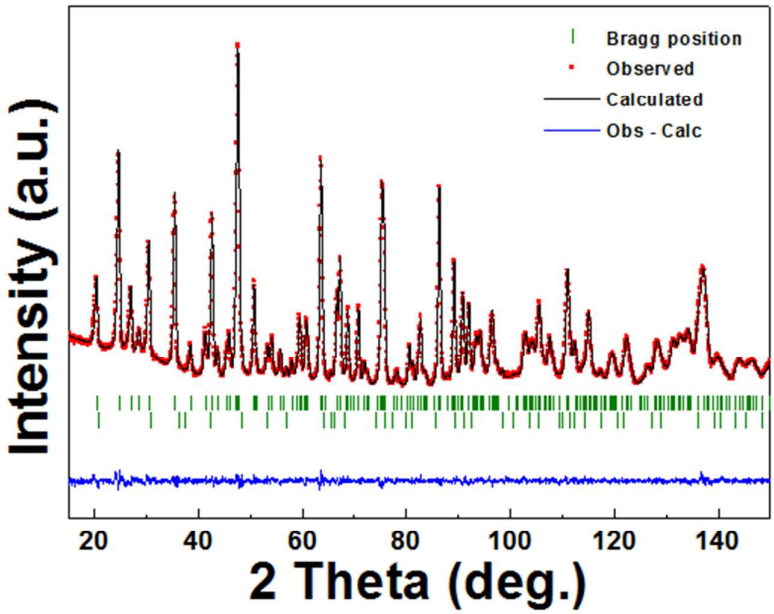

Atom	X	Y	Z	Multi.	Occ.		
Li	0.00000(0)	0.00000(0)	0.00000(0)	4	0.4968(2)	Chi^2	1.33
Fe	0.28207(16)	0.25000(0)	0.9737(5)	4	0.4968(2)	R_p	1.76
Li_{Fe}	0.28207(16)	0.25000(0)	0.9737(5)	4	0.006(2)	R_I	2.23
Fe_{Li}	0.00000(0)	0.00000(0)	0.00000(0)	4	0.006(2)	R_f	0.46
P	0.0952(4)	0.25000(0)	0.4193(7)	4	0.5	Unit cell V.	291.487(19)
O1	0.0977(4)	0.25000(0)	0.7399(6)	4	0.5	Lattice a(Å)	10.32617(38)
O2	0.4569(3)	0.25000(0)	0.2028(7)	4	0.5	Lattice b(Å)	6.00935(24)
O3	0.1640(3)	0.04723(18)	0.2847(5)	8	1	Lattice b(Å)	4.69735(16)

Figure S11. Neutron Rietveld refinement results of solid-state prepared $Li_{0.9}FePO_4$

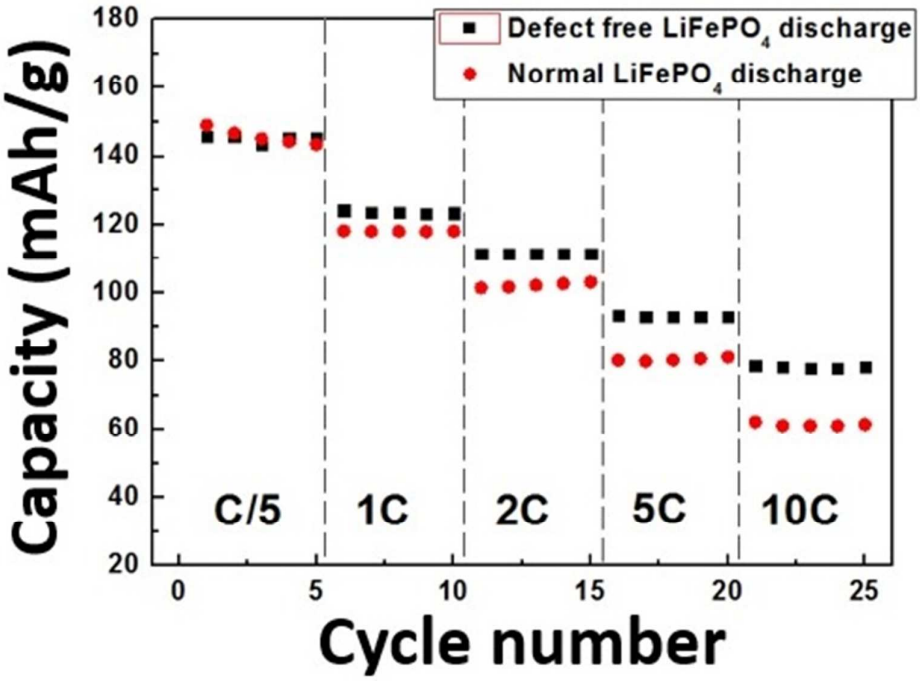

Figure S12. C-rate capability of $LiFePO_4$ (red, prepared by solid-state method without carbon coating) and defect-less $LiFePO_4$ (black, prepared by charge carrier injection method without carbon coating)

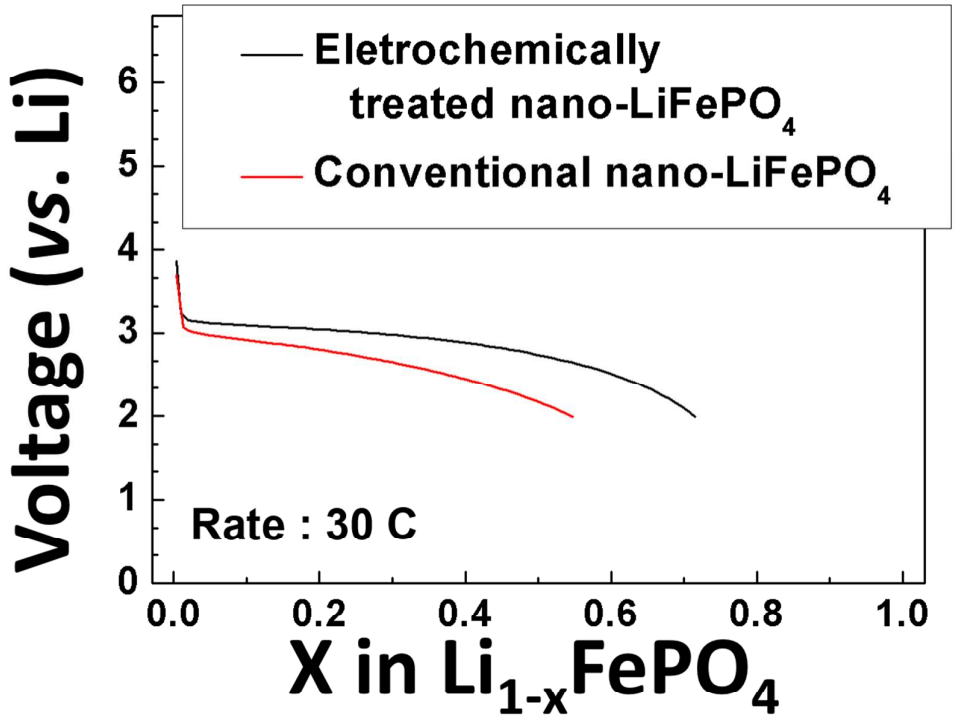

Figure S13. Charge/discharge profile at 30 C of electrochemically treated nano-$LiFePO_4$ and conventional nano-$LiFePO_4$.